metals

Article

Microstructure Evolution Behavior of Spray-Deposited 7055 Aluminum Alloy during Hot Deformation

Di Feng [1,2,3,*], Rui Xu [1], Jichen Li [1], Wenjie Huang [1], Jingtao Wang [2], Ying Liu [2,*], Linxiang Zhao [3], Chengbo Li [4] and Hao Zhang [5]

1 Department of Materials Science and Engineering, Jiangsu University of Science and Technology, Zhenjiang 212003, China
2 Department of Materials Science and Engineering, Nanjing University of Science and Technology, Nanjing 210094, China
3 Suzhou Feihua Aluminum Industry Co., Ltd., Suzhou 215164, China
4 Department of Machinery and Mechanics, Xiangtan University, Xiangtan 411105, China
5 Jiangsu Haoran Spray Forming Alloy Co., Ltd., Zhenjiang 212009, China
* Correspondence: difeng1984@just.edu.cn (D.F.); liuying517@njust.edu.cn (Y.L.); Tel.: +86-0511-8840-1184 (D.F.)

Abstract: The evolution behaviors of the second phase, substructure and grain of the spray-deposited 7055 aluminum alloy during hot compression at 300~470 °C were studied by scanning electron microscopy (SEM), electron backscatter diffraction (EBSD) and transmission electron microscopy (TEM). Results show that the AlZnMgCu phase resulting from the deposition process dissolves gradually with the increase in deformation temperature, but the Al_7Cu_2Fe phase remains unchanged. The plastic instability of the spray-deposited 7055 aluminum alloy occurs at 470 °C with a 1~5 s^{-1} strain rate range. Partial dynamic recrystallization (PDRX) adjacent to the original high angle grain boundaries (HAGBs) not only occurs at 300~400 °C with the low strain rates ranging from 0.001 to 0.1 s^{-1} but also at 450 °C with a high strain rate of 5 s^{-1}. Continuous dynamic recrystallization (CDRX) appears at 450 °C with a low strain rate of 0.001 s^{-1}. The primary nucleation mechanism of PDRX includes the rotation of the subgrain adjacent to the original HAGBs and the subgrain boundary migration. The homogeneous misorientation increase in subgrains is the crucial nucleation mechanism of CDRX. At 300~400 °C, the residual coarse particle stimulated (PSN) nucleation can also be observed.

Keywords: spray deposition; 7055 aluminum alloy; dynamic recovery; dynamic recrystallization

check for updates

Citation: Feng, D.; Xu, R.; Li, J.; Huang, W.; Wang, J.; Liu, Y.; Zhao, L.; Li, C.; Zhang, H. Microstructure Evolution Behavior of Spray-Deposited 7055 Aluminum Alloy during Hot Deformation. *Metals* **2022**, *12*, 1982. https://doi.org/10.3390/met12111982

Academic Editor: Maciej Motyka

Received: 23 October 2022
Accepted: 16 November 2022
Published: 19 November 2022

1. Introduction

Aluminum alloys are widely used in preparing aerospace structural parts due to their high specific strength, excellent corrosion resistance and machinability [1–3]. The Zn/Mg ratio, Zn/Cu ratio and element uniform distribution are the crucial factors determining the service performance of the Al-Zn-Mg-Cu alloy. However, the semi-continuous cast 7055 aluminum alloy has severe composition segregation and a casting cracking tendency [4,5]. Therefore, the primary alloying element content of large-size ingots is limited in the 7055 aluminum alloy. For example, the Zn element is generally set to the lower level of the nominal composition, which restricts the application potential of the Al-Zn-Mg-Cu alloy [6].

Spray deposition is an advanced ingot-forming technology based on rapid solidification [7,8]. In this process, the metal solution is atomized into molten droplets by high-pressure inert gas first. Then, the droplets sputter to a deposition disk at the bottom to form one solidification layer. Finally, a cylindrical ingot can be obtained by stacking layer by layer. During the flight of droplets toward the deposition disc, the cooling rate can reach 10^3 °C/s. Therefore, the dendrite structure is eliminated, and the grain is extraordinarily refined (20–30 μm) by the extreme undercooling degree. More importantly, the alloying elements in the spray-deposited 7055 aluminum alloy have a significant promotion, and there is no macroscopic segregation [9–11]. Therefore, the spray-deposited 7055 aluminum alloy has an extensive application potential for aerospace products.

It should be pointed out that the large size spray-deposited ingot needs to be densified by hot extrusion due to the presence of a certain proportion of "pores" [12,13]. Densification realized by extrusion is also the forming technology of plates and profiles [13,14]. It is well known that the controlling of the recrystallization degree and recrystallized grain size is one of the critical factors in ensuring the mechanical properties and corrosion resistance of the Al-Zn-Mg-Cu alloy. The hot extrusion temperature, extrusion rate and extrusion ratio directly determine the characteristic of the deformation substructure or recrystallized microstructure. In order to bring out the latent potentialities of the finer microstructure and higher element content, it is necessary to investigate the thermal deformation behavior of the spray-deposited 7055 aluminum alloy.

Feng [15] investigated the hot deformation behavior of a Al–7.68 Zn–2.12 Mg–1.98 Cu–0.12 Zr alloy produced by semi continuous casting with a homogenization state. The results revealed that the primary dynamic recrystallization (DRX) mechanism is "the bowing of original grain boundary". The effect of grain size inhomogeneity of the ingot on the dynamic softening behavior of the 7055 aluminum alloy was also researched in detail [16,17]. As mentioned above, the spray-deposited 7055 aluminum alloy showed a finer microstructure, indicating distinctive dynamic softening behaviors. Luo [2] studied the microstructure evolution of the spray-deposited and as-extruded 7055 aluminum alloy during hot compression. However, a detailed and systematic study of the hot deformation behavior, especially the DRX behavior of the as-sprayed 7055 aluminum alloy, has not been reported before.

In this paper, the evolution behavior of the second phase and the grain of the spray-deposited 7055 aluminum alloy was studied by the hot compression test. The dynamic softening mechanism of the rapidly solidified alloy was discussed. Results are also of great significance for the understanding of the thermal deformation behavior and the hot working process optimization of other spray-deposited aluminum alloys.

2. Materials and Methods

The actual composition (mass fraction, %) of the spray-deposited 7055 aluminum alloy ingot is: Zn 8.32, Mg 2.10, Cu 2.24, Zr 0.12, Si 0.030, Fe 0.045 and Al allowance. The specimens of 15 mm in height and 10 mm in diameter were machined from a spray-deposited ingot. The 0.2 mm deep grooves on the end faces were also machined. During compression, the grooves were filled with lubricant to reduce friction. A hot compression test was carried out on the Gleeble-3500 thermal simulator. The specimens were heated to 300 °C, 350 °C, 400 °C, 450 °C and 470 °C within 3 min, respectively, and held for 3 min prior to compression. Then, the specimens were compressed to the required reduction of 60% with the strain rates of 0.001 s^{-1}, 0.01 s^{-1}, 0.1 s^{-1}, 1 s^{-1} and 5 s^{-1}, respectively. Water cooling was conducted immediately after hot compression to freeze the deformed microstructure [18,19].

The grains and dislocations were observed by the TecnaiG^2 20 transmission electron microscope (TEM) and field emission gun scanning electron microscope (SEM) equipped with an electron backscatter diffraction (EBSD) system. The TEM and EBSD specimens were thin foils with the thickness of 80 μm and the diameter of 3 mm, which were electropolished in a solution containing 30%HNO_3 in methanol at ~−25 °C and 15~20 V [17]. On account of the detection limitation in the hot worked structure, boundaries with a misorientation angle of less than 2° were not taken into account for EBSD observation. The EBSD test step size varies from 0.75 to 1.3 μm depending on the substructure scale [20]. The X-ray diffraction (XRD) experiments for the spray deposited specimen and the compressed one were performed on a XRD-6000 X-ray diffractometer using Cu Kα radiation. The measurement step is 1°/min, and the scanning range is 15~90° [21]. MDI Jade 6.5 was used for the qualitative analysis.

3. Results

3.1. True Stress—True Strain Curve

The true stress-strain curves of the spray-deposited 7055 aluminum alloy are shown in Figure 1. Results show that the flow stress increases with the decrease in the deformation temperature or the increase in the strain rate. The steady-state flow stress is only about 10 MPa at 470 °C, 0.001 s^{-1}, while the peak stress can reach 140 MPa at 300 °C, 5 s^{-1}. In addition, the flow stress increases rapidly at the beginning of compression (true strain < 0.1). When the true strain exceeds 0.1, the growth rate of flow stress decreases gradually.

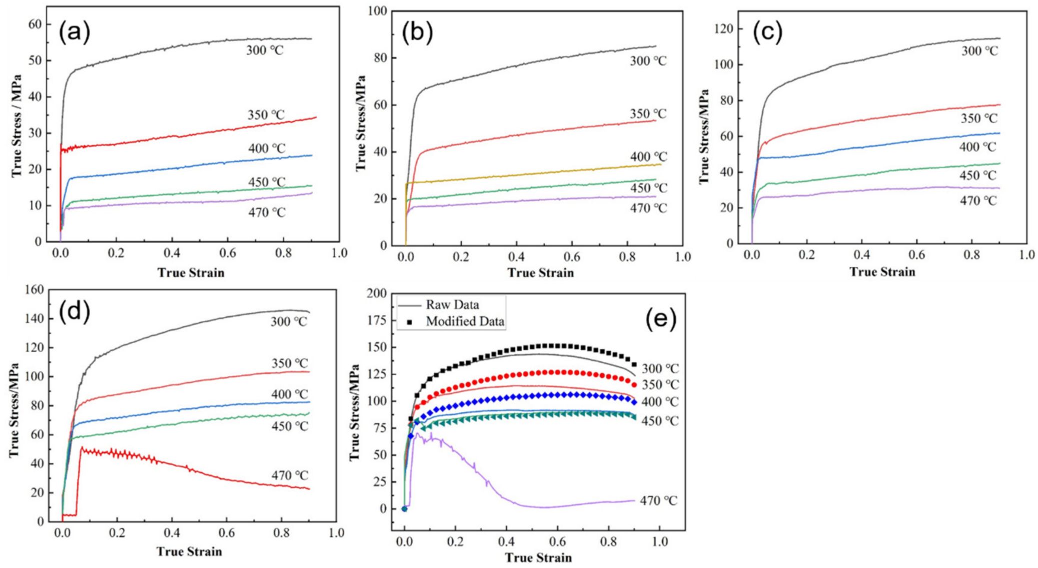

Figure 1. True stress-true strain curves under different strain rate and temperature conditions (Data are corrected based on deformation temperature rise effects for 5 s^{-1} compressed samples) (**a**) 0.001 s^{-1}; (**b**) 0.01 s^{-1}; (**c**) 0.1 s^{-1}; (**d**) 1 s^{-1}; (**e**) 5 s^{-1}.

Under the condition of a low deformation temperature (≤350 °C), it reveals that the flow stress keeps an upward trend with the increase in strain. Taking the hot compression temperature of 300 °C as an example, it can be seen that, from the strain of 0.05 to the completion of hot compression deformation, the flow stress increments ($\Delta\sigma$) at different strain rates are about 10 MPa (0.001 s^{-1}), 20 MPa (0.01 s^{-1}), 35 MPa (0.1 s^{-1}) and 40 MPa (1 s^{-1}), respectively. However, at intermediate and low strain rates (≤1s^{-1}) and temperatures above 400 °C, the stress levels are almost unchanged ($\Delta\sigma$ <10 MPa) after the rapid work hardening. Especially when the deformation temperature reaches 470 °C, the flow stress increment is negligible when the strain is larger than 0.05. It can be concluded that the spray-deposited 7055 aluminum alloy is also sensitive to the deformation temperature and strain rate, and its rheological behavior is more susceptible to the deformation temperature.

The stress-strain curves corresponding to 470 °C and intermediate (1 s^{-1}) and high (≥5 s^{-1}) strain rates decrease sharply after reaching the peak stress. In the process of high-speed thermal deformation, the external input mechanical energy accumulates rapidly by dislocation multiplication. The DRX behavior can effectively reduce the dislocation density and avoid the material fracture caused by severe work hardening. However, at a higher deformation temperature (470 °C), the temperature rise caused by the high strain rate exceeds the melting point of eutectic structures on the grain boundary, which eventually leading to the intergranular fracture. Therefore, it is preliminarily concluded that the deformation temperature of the spray-deposited 7055 aluminum alloy should not exceed 450 °C in the rapid deformation process, such as forging.

3.2. Deformation Microstructure Analysis

3.2.1. The Second Phase

Figure 2 shows the microstructure of as-sprayed and as-compressed states, respectively. It can be seen that the volume fraction of the white coarse second phase in the as-deposited specimen is the highest. The length-thickness ratio of the second phase inside the grain is small and evenly distributed. However, the ones on the grain boundary have a larger length-thick ratio. The coarse phases distribute along the grain boundary, outlining the morphology of the equiaxed grain (Figure 2a). Besides, the arrangement of the second phase in the as-sprayed specimen has no directivity.

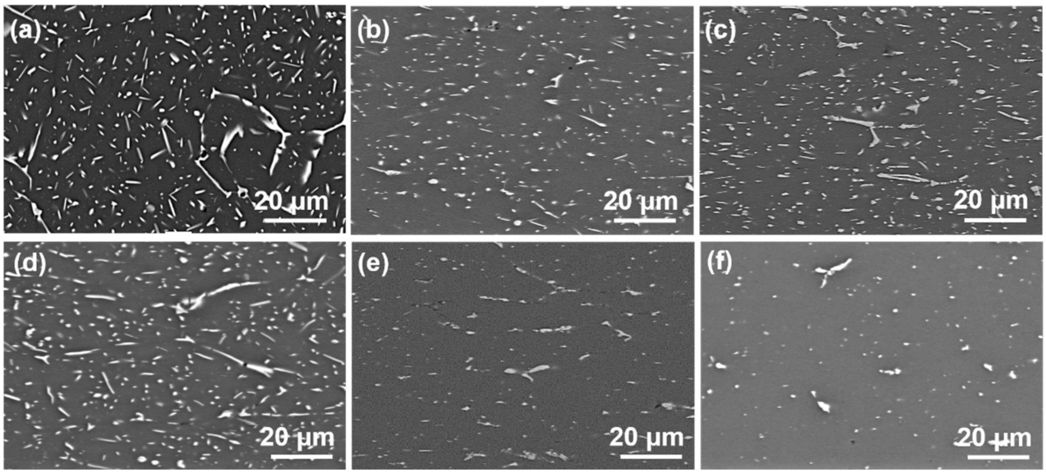

Figure 2. SEM images of 7055 aluminum alloy under spray-deposited state (**a**), 300 °C/5 s^{-1} (**b**), 300 °C/0.001 s^{-1} (**c**), 400 °C/0.1 s^{-1} (**d**), 450 °C/5 s^{-1} (**e**) and 450 °C/0.001 s^{-1} (**f**).

With the increase in the hot compression temperature or the decrease in the strain rate, the volume fraction of the coarse second phase decreases gradually. Image J software was used to calculate the area fraction of the second phase. Results show that, after hot compression at 300 °C (Figure 2b,c), the area fraction of the second phase is about 13%. The number of the intragranular phase decreases significantly, while the grain boundary phase remains unchanged. When the deformation temperature is 400 °C, the total area fraction decreases to about 8% (Figure 2d). The length-thickness ratio also reduces significantly. When the deformation temperature rises to 450 °C, the area fraction of the second phase in the specimen deformed at 5 s^{-1} is only about 2% (Figure 2e). However, the second phase in the specimen deformed at 0.001 s^{-1} almost dissolves completely. The residual phases on the grain boundary also spheroidize and coarsen (Figure 2f).

The element plane scanning results under different deformation conditions are shown in Figure 3. It reveals that the residual second phases are mainly AlZnMgCu quaternary particles (Figure 3a–e). Fe-containing phases also exist (Figure 3a,c). The type of the second phase remaining after hot compression is consistent with that of the as-deposited state. The Fe-containing phase is the crystalline phase formed in the deposition process and cannot be dissolved by heat treatment or thermal deformation.

The literature [22] shows that when the deformation temperature rises to 400~450 °C, the Fe-containing phase is exposed due to the dissolution of the associated AlZnMgCu phase. This coarse second phase will hinder the dislocation movement during thermal deformation, thus affecting the evolution behaviors of the substructure or the migration of high angle grain boundaries (HAGBs) during recrystallization.

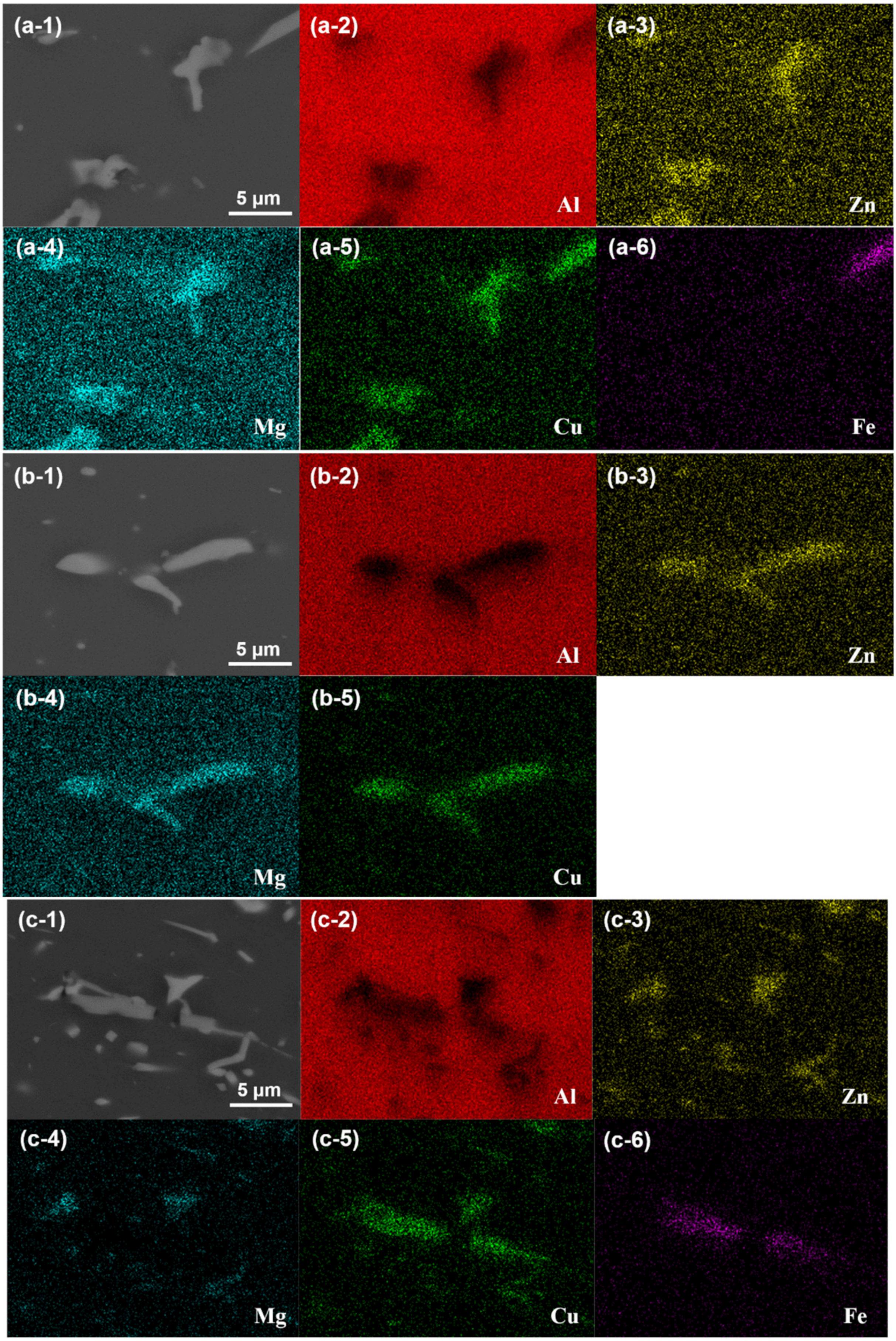

Figure 3. *Cont.*

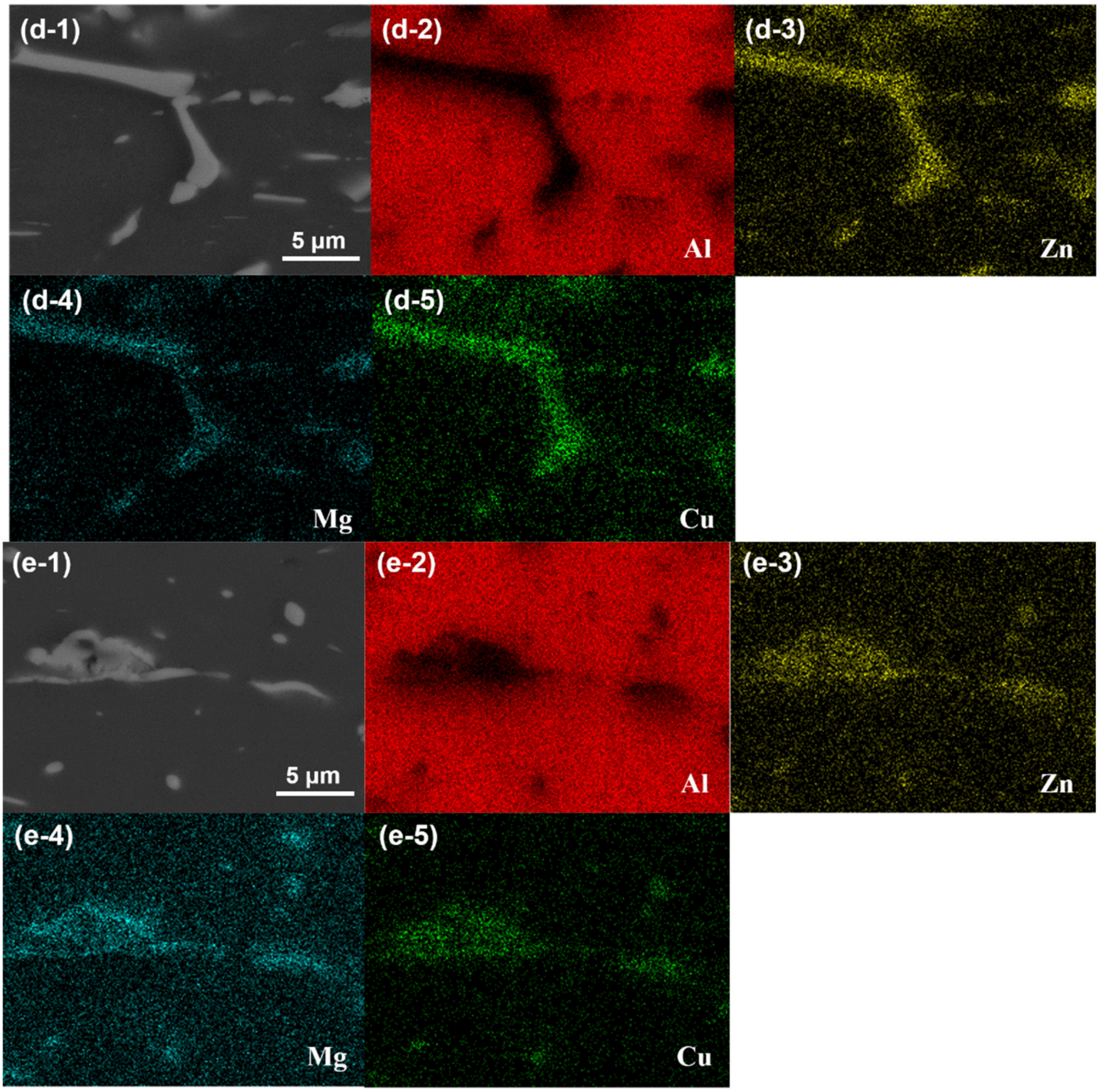

Figure 3. Element plane scanning images of the second phase of spray-deposited 7055 aluminum alloy under hot compression conditions of 450 °C/0.001 s^{-1} (**a**), 450 °C/5 s^{-1} (**b**), 400 °C/0.1 s^{-1} (**c**), 300 °C/0.001 s^{-1} (**d**) and 300 °C/5 s^{-1} (**e**).

The XRD patterns of the spray-deposited specimen and the one hot compressed under 450 °C/0.001s^{-1} are shown in Figure 4. It is depicted that the AlZnMgCu phase has the same crystal structure as $MgZn_2$ [23]. Based on EDS, we know the second phase also contains Al and Cu. So, the AlZnMgCu phase can also be defined as the Mg $(Zn,Cu,Al)_2$ phase [24]. Besides, the AlZnMgCu phase or Mg $(Zn,Cu,Al)_2$ phase decreases with the increase in the compressed temperature and the decrease in the strain rate, which is consistent with the SEM analysis results.

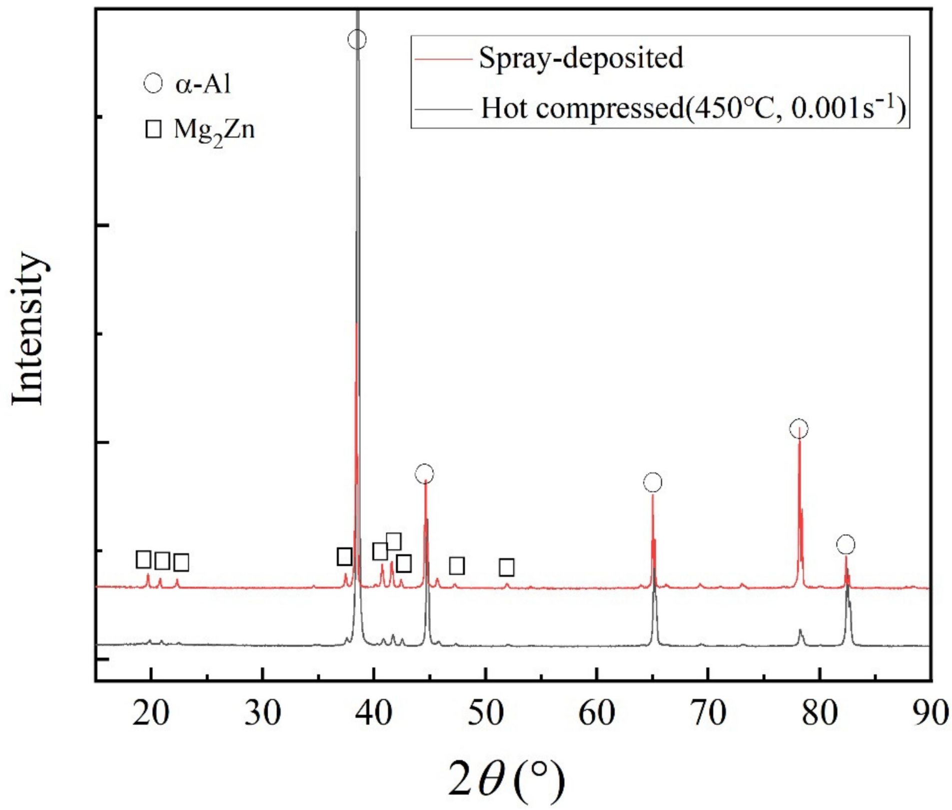

Figure 4. The XRD patterns of the spray-deposited specimen and the one deformed under 450 °C/0.001 s^{-1}, respectively.

3.2.2. Grain Morphology

Figure 5 shows the EBSD images of the hot compressed alloy before and after compression. The grains of the as-spray-deposited state are equiaxed (as shown in Figure 5a), and the size ranges from 20 to 50 μm. After deformed at the low temperature of 300 °C and a high speed of 5 s^{-1} (as shown in Figure 5b), the original equiaxed grain is compressed into a flat shape with a high-density deformation substructure inside. A small number of fine equiaxed recrystallized grains with a size range of only 3~5 μm can be observed at the original HAGBs. When the strain rate decreases to 0.001s^{-1} (Figure 5c), the size of recrystallized grains at HAGBs increases to 5~10 μm. The average size of the deformed substructure increases to about 10 μm. When the deformation temperature increases to 400 °C, the size of DRX grains and deformation substructures continue increasing (> 10 μm), as shown in Figure 5d. At the deformation temperature of 450 °C, the fine DRX grains distributed continuously on the grain boundaries disappear. Equiaxed DRX grains with the large size range of 10~50 μm can be observed at the trigeminal grain boundaries (Figure 5e). The volume fraction of the substructure decreased significantly, and some subgrains even grew to a scale of 50 μm (Figure 5f).

According to the above analysis, the primary dynamic softening mechanism of the spray-deposited 7055 aluminum alloy under low temperatures is dynamic recovery (DRV). The limited DRX microstructure is characterized by small-size equiaxed grains with a pearl necklace shape at the original HAGBs. Therefore, the dynamic softening effect under a low temperature is limited. When the dislocation multiplication is quicker than annihilation, the flow stress will continue rising slowly, as shown in the stress-strain curve under the 300 °C deformation condition in Figure 1.

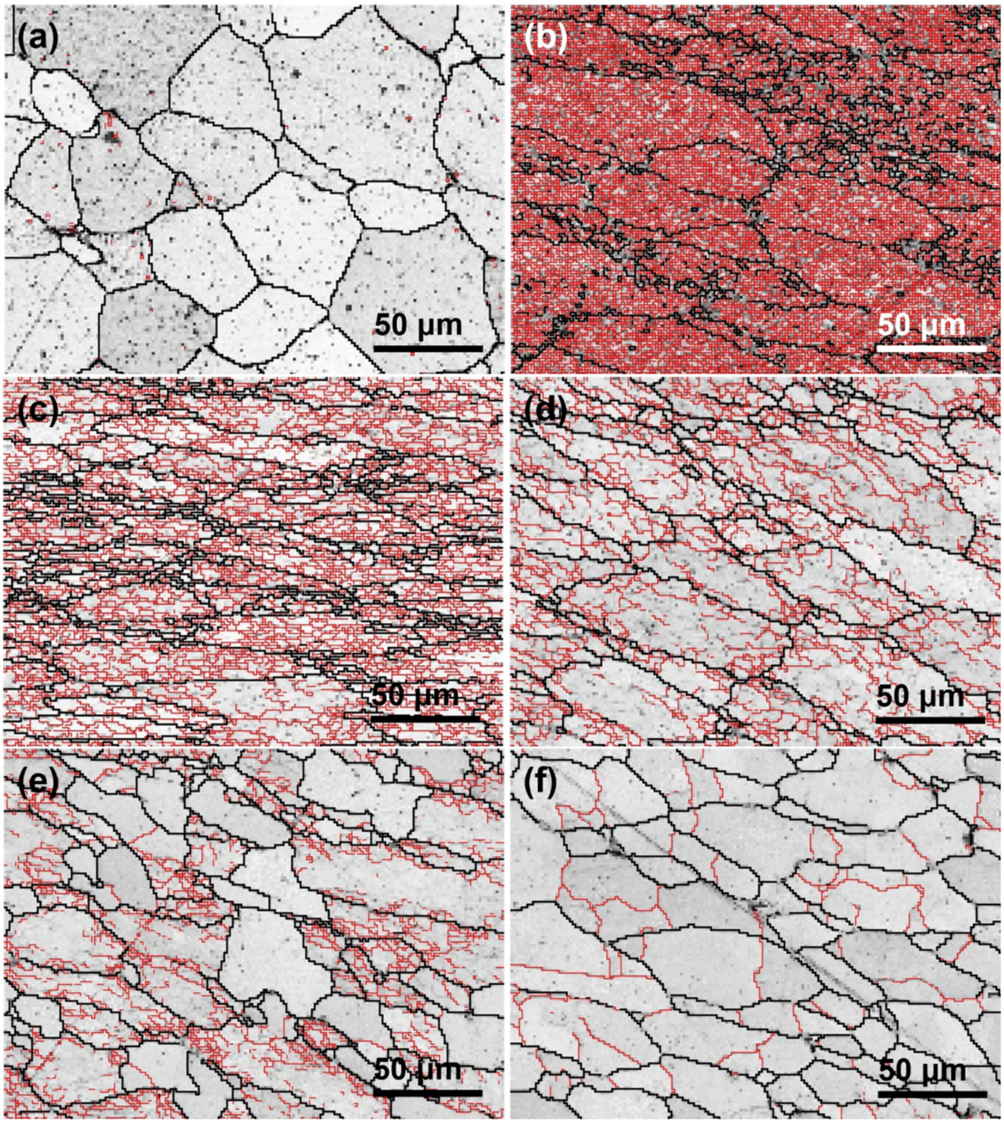

Figure 5. EBSD images of grain morphology of spray-deposited 7055 aluminum alloy (**a**) and under hot compression conditions of 300 °C/5 s^{-1} (**b**), 300 °C/0.001 s^{-1} (**c**), 400 °C/0.1 s^{-1} (**d**), 450 °C/5 s^{-1} (**e**) and 450 °C/0.001 s^{-1} (**f**) (Black line represents the high angle grain boundaries (HAGBs) which are higher than 15°, and the red line represents the low angle grain boundaries (LAGBs) ranging from 2° to 15°).

The Zener–Hollomon (Z) parameter is described as the temperature-compensated strain rate factor. The value of Z decreases with the decrease in the strain rate or the increase in the deformation temperature. With the decrease in the Z value, the DRX degree, the DRX grain size and the subgrain size all increase gradually, but the substructure volume fraction decreases. When compressed at 450 °C, the equiaxed DRX grains replace the original ones (Figure 5e,f). It can be concluded that the spray-deposited 7055 aluminum alloy undergoes almost complete DRX during compression at 450 °C. Due to the sufficient growth of the substructure under high-temperature conditions, the DRX nucleation should be dominated by the progressive transformation of subgrains. The DRX grains also grow sufficiently under low strain rates, as shown in Figure 5f.

3.2.3. The Substructures

Figure 6 shows the substructures of the as-deformed specimens of the 7055 aluminum alloy. In addition to the micron-level second phase, there are also amounts of smaller second phases with the size of 200~300 nm. At 300 °C, the density of the second phase and deformation substructure is highest in the specimen deformed with $5s^{-1}$, and the substructure size is the smallest (ranging from 0.5 to 2 μm). It is worth noting that the average size of the subgrains is almost the same as that of the residual coarse phase, as shown in Figure 6a. With the decrease in the *Z* parameter, the subgrain size increases. The average size of the subgrains ranges from 5 to 8 μm in the specimen deformed at 300 °C with 0.001 s^{-1}. The residual coarse second phase distributes on the subgrain boundary (Figure 6b). Low-density dislocation entanglement also exists in subgrains.

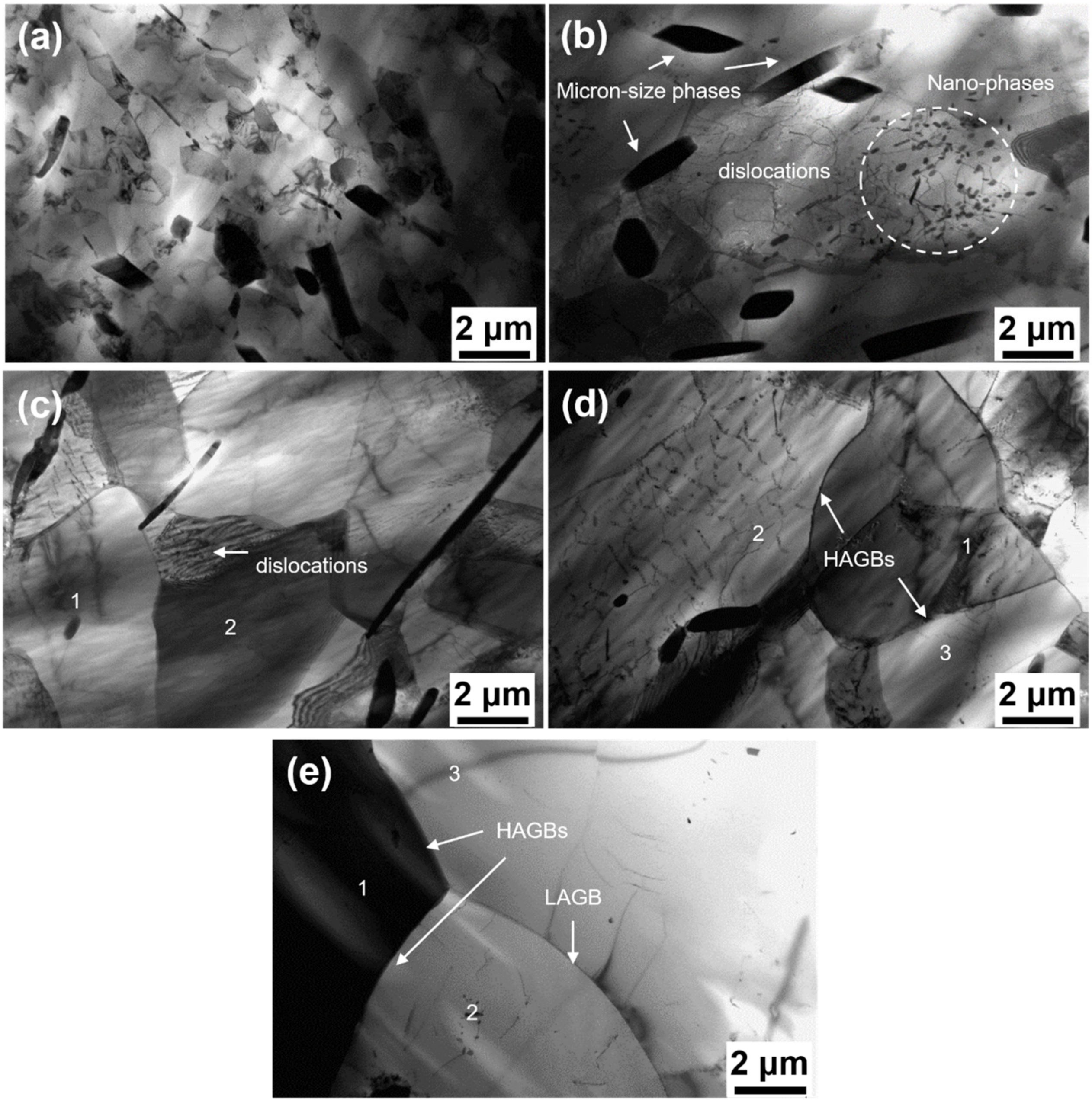

Figure 6. TEM images of the sub-microstructure of spray-deposited 7055 aluminum alloy under hot compression conditions of 300 °C/5 s^{-1} (**a**), 300 °C/0.001 s^{-1} (**b**), 400 °C/0.1 s^{-1} (**c**), 450 °C/5 s^{-1} (**d**) and 450 °C/0.001 s^{-1} (**e**).

At 400 °C/1 s^{-1} and 450 °C/5 s^{-1} deformation conditions, only a very small amount of the micron second phase remains (Figure 6c). The subgrains develop maturely and some dislocation-free subgrains can be observed (Figure 6d). In some grains, dislocation entanglement and cellular structure can also be observed. The dynamic softening behavior consumes deformation energy storage through dislocation slip and climbing, and even results in DRX. However, the dynamic hardening behavior constantly introduces dislocations, and the new dislocations cannot be consumed by the growth of substructures in time. Therefore, sufficient subgrain growth and dislocation entanglement coexists in thermally deformed samples. In addition, large-size subgrains 1 and 2 or 3 have an obvious contrast under the same incident condition (Figure 6d), which indicates that the grain boundary between grains 1 and 2 or 1 and 3 has large misorientation. That means grain 1 was a recrystallized nucleus or will grow into the nucleus if the deformation continues.

Under the 450 °C/0.001 s^{-1} deformation condition, the second phase of the micron size is completely dissolved. As depicted in Figure 6e, the misorientation between large subgrains 1 and 2 or 1 and 3 was more prominent, which indicates that the flat interface between grains 1 and 2 or 1 and 3 should also be HAGB. The large subgrain 1 developed into a DRX nucleus. Besides, the subgrain boundary between grains 2 and 3 shows a large curvature. It can be inferred that grains 2 and 3 will eventually develop into another DRX nucleus by subgrain boundary migration. In addition, at 450 °C, few residual dislocations were observed in the 0.001 s^{-1} deformed specimen. Unlike the high-speed deformed samples at 450 ° C, the strain rate of 0.001 s^{-1} is very low, so the new dislocations have enough time to be consumed by substructure growth or recrystallization nucleation (Figure 6e).

4. Discussion

As we all know, the fault energy γ_{SFE} determines the extent to which unit dislocations dissociate into partial dislocations. For materials with high γ_{SFE}, such as aluminum (166 mJ·m^{-2}), the dissociating of the dislocation into two partials is more difficult. Therefore, it is generally believed that Al-Zn-Mg-Cu alloys mainly undergo DRV during hot deformation, and only partial DRX occurs under the condition of a low Z value [25]. Because most of the DRX grains appear adjacent to the original HAGBs, the primary DRX nucleation theories of the 7055 aluminum alloy are "strain-induced HAGB migration (SIBM)" and "subgrain rotation near HAGBs". It should be noted that the content of alloying elements of the high-strength 7000 series aluminum alloy can exceed 20% (mass fraction). The fault energies of Zinc, Magnesium and Copper are 140, 74~125 and 78 mJ·m^{-2} [25,26], respectively. Studies [26,27] show that the co-addition of these alloying elements can effectively reduce the fault energy of the aluminum alloy, and then affect the movement behavior and the dislocation configuration, resulting in a dynamic softening mechanism different from that of pure aluminum. In addition, the interaction between a large number of micron-scale second phases and dislocations will also change the configuration of dislocations, thus enriching the dynamic softening behavior.

4.1. Interaction between the Second Phase and Dislocation

The residual coarse phases ranging from 1 to 2 μm under different Z parameters are depicted in Figure 7. It can be seen from Figure 7a that there are a lot of fine sub-structures and cellular structures when deformed at 300 °C with 5 s^{-1}. This typical DRV behavior can be explained as follows: on the one hand, there is no time and a lack of thermal activation to obtain an adequate annihilation or rearrangement degree of dislocations. On the other hand, due to the pile-up of dislocations in front of the large second phase, a rapid formation of sub-microstructures can be stimulated by the dislocation packing. A different contrast indicates a large misorientation between subgrains 1 and 2. The right side of subgrain 1 is close to the residual coarse second phase. The high-density dislocation configuration in front of the second phase will produce a subgrain with relatively large misorientation.

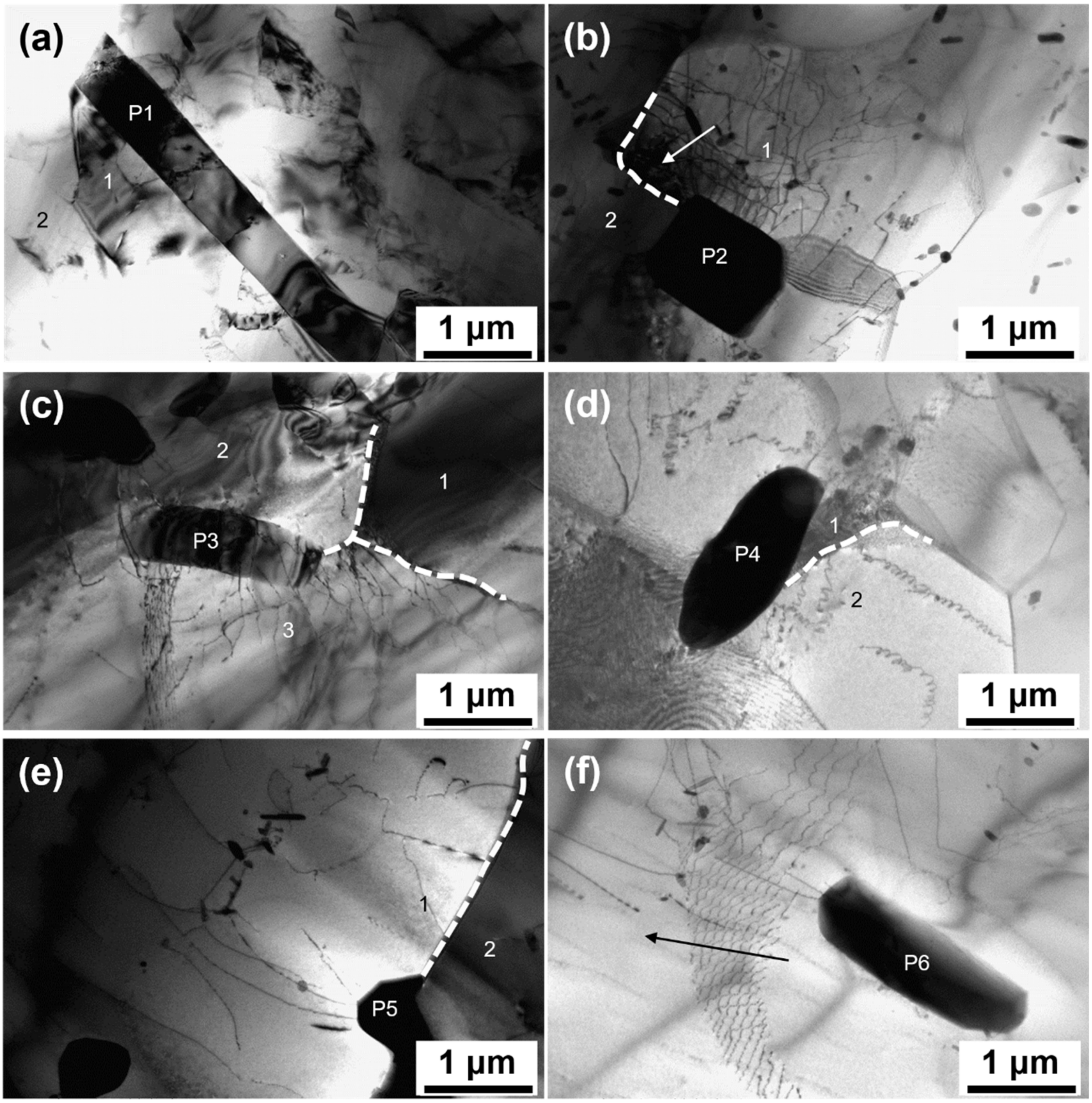

Figure 7. TEM images of interaction between dislocation and second phase of spray-deposited 7055 aluminum alloy under hot compression conditions of 300 °C/5 s^{-1} (**a**), 300 °C/0.001 s^{-1} (**b**), 400 °C/0.1 s^{-1} (**c**), 450 °C/5 s^{-1} (**d**) and 450 °C/0.001 s^{-1} (**e**,**f**); P_i (i = 1~6) represents the particles that remained after hot compressed.

In Figure 7b, the dislocation entanglement can be observed at the front of the second phase (the area pointed by the arrow). The local interface (dotted line) between subgrains 1 and 2 continuously absorbs the stacking dislocations, resulting in a misorientation increase. When the subgrain boundary evolves to a HAGB, DRX nucleation completes. In Figure 7c, there is a particle P3 between subgrains 2 and 3. Subgrain 1 has no contact with P3. Therefore, the misorientation between subgrains 2 and 3 is discernible, while that between subgrains 2/3 and 1 is relatively larger. In Figure 7d, the dislocation density decreases significantly due to the high compression temperature. The grain boundary of subgrain 2 continuously absorbs the lattice dislocations near the P4 to increase its misorientation, and finally evolves into a HAGB. Figure 7e,f show the second phase morphology on the grain boundary and inside the grain of the specimen deformed at 450 °C with 0.001 s^{-1}, respectively. The residual second phase inner grain serves as the source of dislocation generation, providing dislocations to the grain boundary (the arrow represents the direction of the dislocation slip). At this time, the climbing ability of dislocation is enhanced. There is enough time to finish polygonization and annihilation. Therefore, the dislocation stacking at the front of the second phase or the grain boundary is insignificant anymore.

It can be concluded that, under high Z value conditions, the volume fraction of the residual second phase increases. The dislocation climbing and cross slip capabilities are restricted. Under this condition, the interaction behaviors between the second phase and dislocations consist of "dislocation entanglement" and "dislocation-packing induced subgrains forming" in front of the second phase. There is a relatively large misorientation between the subgrains near the second phase and those faraway. At low Z values, the volume fraction of the residual second phase decreases. Dislocations are thermally activated without being effectively blocked.

4.2. Dynamic Recovery Behavior

It can be seen from Figure 8 that the substructure size increases with the decrease in Z. At 300 °C, there are dislocation cells (<1μm) in the specimen deformed with 5 s^{-1}. The left side of the cell boundary is composed of the dislocation wall (the white dotted line), while the right side retains a high-energy dislocation network. Under the high strain rate and low temperature conditions, it is a lack of time for the dislocation migrating to the cell boundary. The 300 °C/0.001 s^{-1} deformed specimen also has the dislocation wall. The walls form a "Y" shape, which divides one substructure into three parts. However, the dislocation network cannot be observed in segmented intracellular regions. Compared with the deformed sample at 300 °C with 5 s^{-1}, the dislocations have enough time to construct a low-energy configuration. The remaining scattered dislocations inside the cell will also continue to slip into the dislocation wall. Annihilation of unlike dislocations and the rearrangement of dislocations coexist. Thus, the density of dislocations with the same type increases in the dislocation wall. The grain boundary misorientation increases continuously.

At 400 °C/0.1 s^{-1} and 450 °C/5 s^{-1} conditions, the substructures with the size of 1~2 μm are dislocation-free. Part of the boundary of this substructure is flat and sharp (as shown by the white dashed line in Figure 8c,d) and has evident misorientation to the adjacent microstructure. Another part of the interface of this structure is characterized by low-density interfacial dislocations. These mobile dislocations are consuming the adjacent dislocation network through interfacial migration, as shown by the arrows.

It can be concluded that this kind of substructure has almost finished the transformation to the subgrain. The subgrains 1 and 2 in Figure 8c,d will grow sufficiently by the local interface migration. As shown in Figure 8e, the subgrains in the sample deformed at 450 °C/0.001 s^{-1} grew completely, and their size can reach a scale of tens of microns. The few remaining dislocations in the subgrain arrange to a low energy state and tend to merge into the subgrain boundary.

4.3. Dynamic Recrystallization Behavior

Dynamic recrystallization requires higher thermal activation. EBSD analysis reveals that there is no apparent DRX in the 300 °C/5 s^{-1} deformed specimen. DRX nuclei of specimens deformed at 300 °C/0.001 s^{-1}, 400 °C/0.1 s^{-1}, 450 °C/5 s^{-1} and 450 °C/0.001 s^{-1} are shown in Figure 9. The size of the recrystallized nucleus ranging from 8 to 10 μm is larger than that of the DRV substructure. In the 300 °C/0.001 s^{-1} condition, the dislocation-free subgrains containing a coarse second phase can be observed (as shown in the solid line frame in Figure 9a). Similar features also appear in specimens deformed at 400 °C/0.1 s^{-1} (solid line frame in Figure 9b). Research shows that the particle-stimulated nucleation (PSN) occurs during the static recrystallization of cold-deformed metals [27]. Similarly, under the condition of a high temperature and large strain (the compression in this experiment is 60%), the DRX based on PSN can also be observed. Zang [28] et al. studied the hot deformation behavior of the Al-7.9 Zn-2.7 Mg-2.0 Cu alloy sheet during the hot rolling process. The results show that the residual coarse second phase after homogenized heat treatment can also produce particle excitation nucleation.

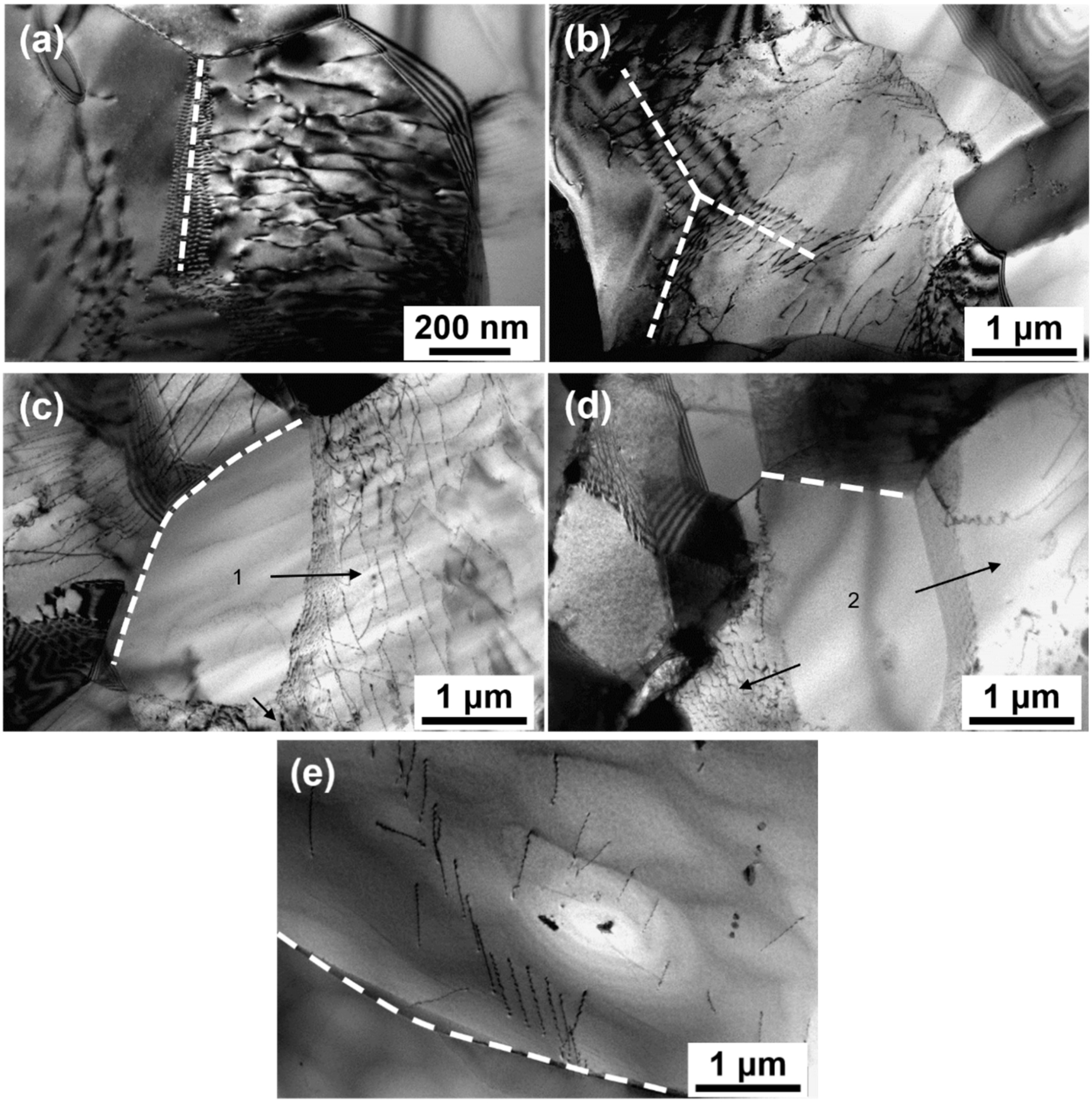

Figure 8. TEM images of DRV microstructure of spray-deposited 7055 aluminum alloy under hot compression conditions of 300 °C/5 s^{-1} (**a**), 300 °C/0.001 s^{-1} (**b**), 400 °C/0.1 s^{-1} (**c**), 450 °C/5 s^{-1} (**d**) and 450 °C/0.001 s^{-1} (**e**).

Subgrains with a large curvature and HAGBs can be observed in the 400 °C/0.1 s^{-1} and 450 °C/5 s^{-1} deformed specimens. The local grain boundaries of the subgrains are bulging out to the high-density dislocation (depicted by the arc-shaped grain boundaries and migration arrow directions in Figure 9b,c). The dislocation network will be swept by the bulging of the subgrain boundary. Then, the misorientation increases continuously, eventually forming the recrystallized nucleus. It indicates that subgrain boundary migration is also the DRX nucleation mechanism of the spray-deposited 7055 aluminum alloy. Under the deformation condition of 450 °C/0.001 s^{-1}, the polygonal recrystallized nuclei with flat grain boundaries appeared (the grains 1 and 2 shown in Figure 9d). There is also a small subgrain at the grain boundary triple junctions between grains 1, 2 and 3. Under the migration of grain boundaries of grains 1 and 2, the small subgrain will disappear. It is a typical characteristic of the nucleation mechanism named "subgrain boundary migration".

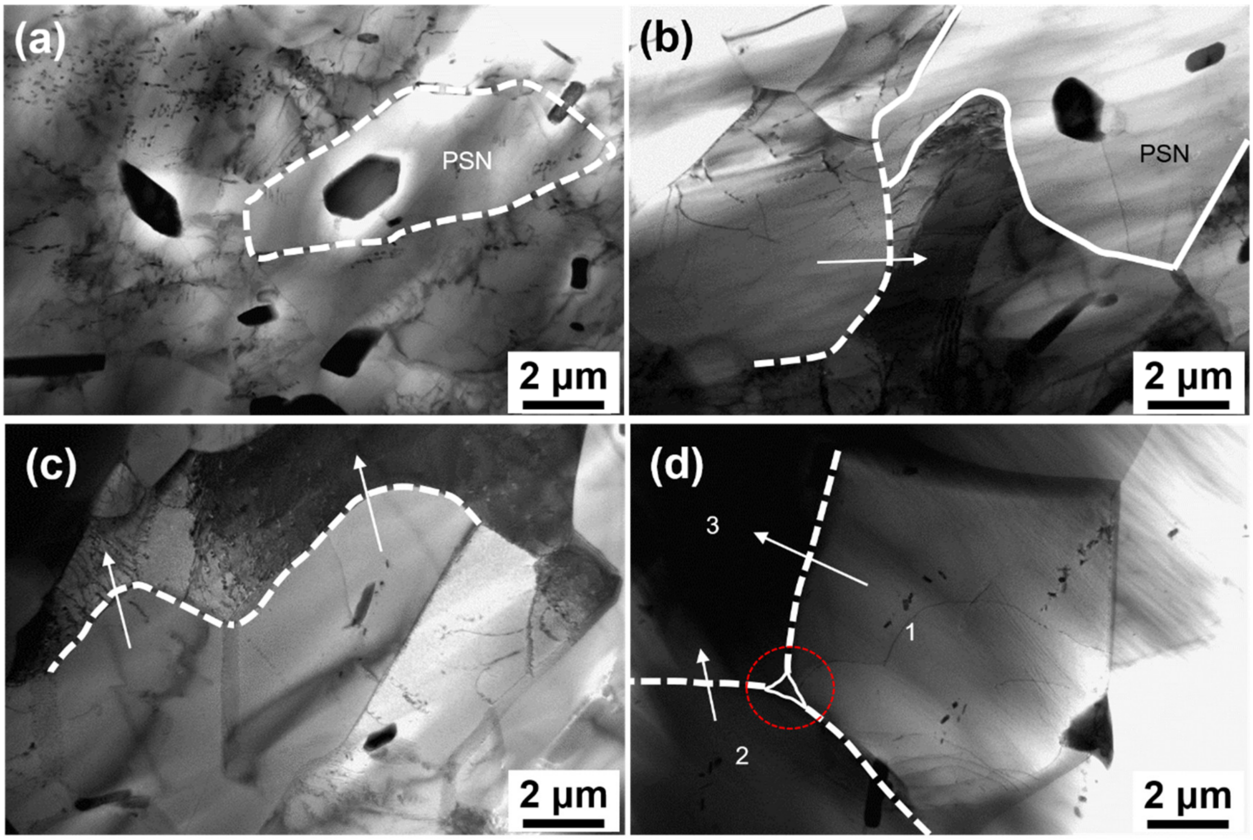

Figure 9. TEM images of DRX microstructure of spray-deposited 7055 aluminum alloy under hot compression conditions of 300 °C/0.001 s^{-1} (**a**), 400 °C/0.1 s^{-1} (**b**), 450 °C/5 s^{-1} (**c**) and 450 °C/0.001 s^{-1} (**d**).

Figure 10 shows the inverse pole figure (IPF) diagrams of the spray-deposited 7055 aluminum alloy under different hot compression conditions. Figure 11 shows the statistics of cumulative misorientation of subgrains along the arrows shown in Figure 10. Under different Z parameters, the accumulative misorientations from the interior grain to the HAGBs all indicate a significant increase in misorientation (12~20 °). Research shows that "subgrain rotation near original grain boundary" occurs when the cumulative misorientation in the grain exceeds 10°. The so-called subgrain rotation mechanism can be described as follows: There is a small misorientation between two adjacent subgrains. The dislocation network on the subgrain boundary can be dissociated, disassembles and transfers to the adjacent subgrain boundary, resulting in the disappearance of the subgrain boundary, and then a nucleus formed. Since favorably slip systems are always activated adjacent to the HAGBs, it is easier to create a recrystallized nucleus when the subgrain rotation occurs at the front of the original HAGBs. This also explains why dynamic recrystallization occurs preferentially at the original grain boundary, as shown in Figure 10a. With the decrease in the Z parameter, the recrystallized nucleus grows up and nucleates again at the newly formed HAGB. Therefore, the DRX characteristics as a necklace at the original grain boundary become less evident with the decrease in the Z parameter, as shown in Figure 10b–d.

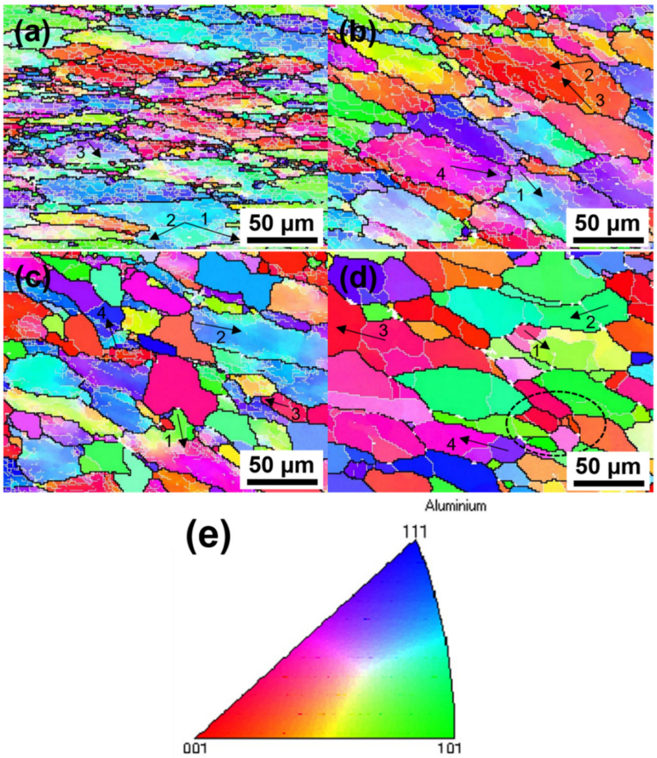

Figure 10. IPF images of the deformed microstructure of spray deposited 7055 aluminum alloy under hot compression conditions of 300 °C/0.001 s^{-1} (**a**), 400 °C/0.1 s^{-1} (**b**), 450 °C/5 s^{-1} (**c**) and 450 °C/0.001 s^{-1} (**d**). (**e**) Representation of the color code used to identify the crystallographic orientation on a standard stereographic (Arrows 1, 2, 3 and 4 in each image are the misorientation cumulative routes).

Besides, at relatively high temperatures, a homogeneous microstructure usually develops (Figure 5e,f). Research reported that the CDRX occurs by the progressive accumulation of dislocations into the low angle grain boundaries (LAGBs) which increase the misorientation. Eventually, HAGBs are formed when the misorientation reaches a critical value of about 15°.

As shown in Figure 10d, several fine recrystallized grains gather together (in the dashed box). This characteristic is not only different from the result after the subgrain rotation but also different from the result of the subgrain boundary migration, indicating a progressive misorientation increase in subgrains.

Figure 12 is a diagrammatic sketch of microstructure evolution. The microstructure evolution of the spray-deposited 7055 aluminum alloy can be divided into three cases: (1) DRV behavior at a low temperature and high strain rate. The second phase is less dissolved. High-density and small-size subgrains appear; (2) DRV and DRX behaviors at an intermediate strain rate and temperature. The amount of the second phase dissolved increases with the increase in the deformation temperature. However, there is still a small amount of an undissolved and large-sized second phase, resulting in particle stimulated nucleation (PSN). There is also subgrain boundary migration nucleation inside the grains. However, the primary recrystallization nucleation mechanism is the subgrain rotation at the HAGBs; (3) Almost complete dynamic recrystallization occurs at high temperatures and low strain rates. In this condition, the subgrains are well defined first. Recrystallization nuclei are formed by the mechanism of the homogeneous misorientation increase, which can be considered as continuous dynamic recrystallization.

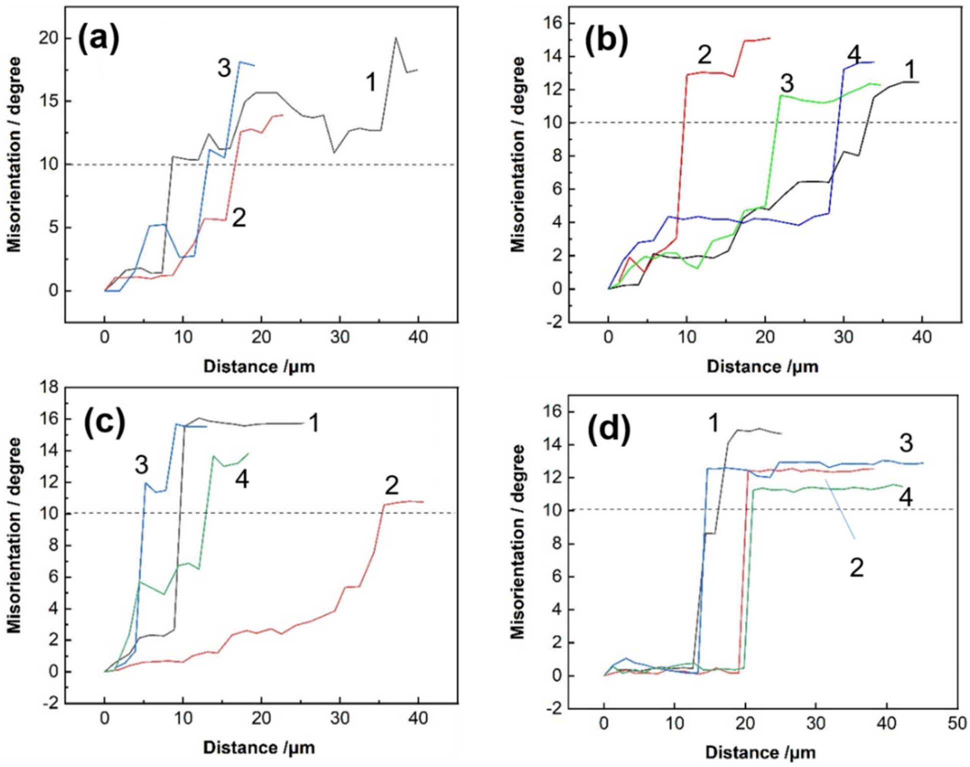

Figure 11. Misorientation cumulative images between deformed subgrains of spray-deposited 7055 aluminum alloy under hot compression conditions of 300 °C/0.001 s^{-1} (**a**), 400 °C/0.1 s^{-1} (**b**), 450 °C/5 s^{-1} (**c**) and 450 °C/0.001 s^{-1} (**d**). (Curves 1, 2, 3 and 4 in each image are the misorientation cumulative routes in Figure 10).

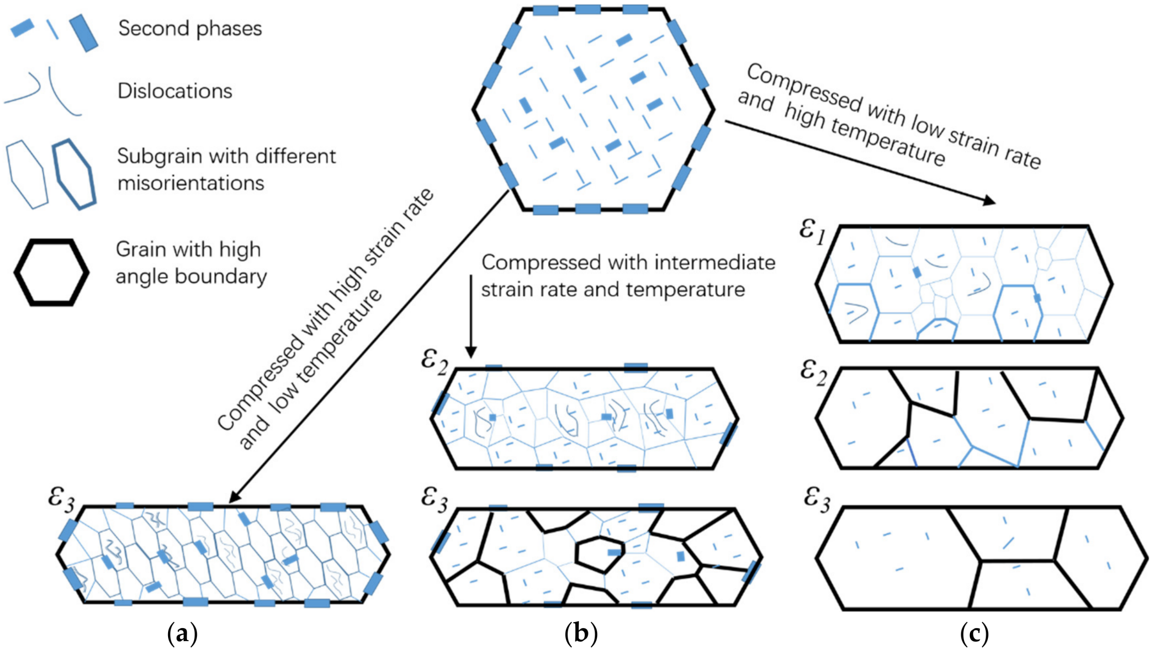

Figure 12. Diagrammatic sketch of the microstructure evolution of spray-deposited 7055 aluminum alloy. (**a**) Dynamic recovery and a few second phases resolve. (**b**) Dynamic recrystallization based on the "subgrain rotation", "subgrain boundary migration" and "PSN" nucleated mechanism. (**c**) Dynamic recrystallization based on "homogeneous misorientation increase of subgrain", and a few phases exist.

When compared with the dynamic recrystallization behavior of the 7055 aluminum alloy produced by semi-continuous casting [16,17], the spray-deposited 7055 aluminum alloy showed the complex DRX mechanisms and a higher DRX degree, which are beneficial to reduce the deformation resistance and improve the deformation ability.

5. Conclusions

(1). The AlZnMgCu phase in the spray-deposited 7055 aluminum alloy gradually dissolves with the increase in the deformation temperature, while the Al_7Cu_2Fe phase does not change. The residual AlZnMgCu phase can induce the rapid formation of subgrains and produce particle stimulated nucleation (PSN) recrystallization.
(2). The plastic instability of the spray-deposited 7055 aluminum alloy occurs at 470 °C with 1~5 s^{-1} strain rates. DRV and DRX occur under other strain conditions simultaneously. The DRX behavior is evident at low *Z* parameters.
(3). The DRX nucleation mechanism at 300~400 °C and 0.001~0.1 s^{-1} is "subgrain rotation near the original HAGBs" and "subgrain boundary migration". Under a 450 °C deformation temperature with a low strain rate, the nucleation mechanism is considered "the homogeneous misorientation increase of subgrain". At the high strain rate of 300~400 °C, "residual coarse second phase particle stimulated nucleation" also occurs.

Author Contributions: Investigation, Methodology, Data Curation, Writing—original draft, D.F. and R.X.; Resources, Conceptualization, Formal analysis, Writing—review and editing, J.L. and W.H.; Conceptualization, Data curation, C.L. and Y.L.; Funding Acquisition, H.Z.; Validation, Supervision, J.W. and L.Z. All authors have read and agreed to the published version of the manuscript.

Funding: This research was funded by the National Natural Science Foundation of China (grant No.52205421), the Key Research and Development Program of Zhenjiang City (grant Nos. GY2021003 and GY2021020), Graduate Research and Innovation Projects in Jiangsu Province (grant No.KYCX21_3453) and Undergraduate Innovation and Entrepreneurship Training Program of Jiangsu Province (grant No.202210289112Y).

Institutional Review Board Statement: Not applicable.

Informed Consent Statement: Not applicable.

Data Availability Statement: Not applicable.

Acknowledgments: The authors would like to appreciate the financial supports from the National Natural Science Foundation of China (grant No.52205421), the Key Research and Development Program of Zhenjiang City (grant Nos. GY2021003 and GY2021020), the Graduate Research and Innovation Projects in Jiangsu Province (grant No.KYCX21_3453) and the Undergraduate Innovation and Entrepreneurship Training Program of Jiangsu Province (grant No.202210289112Y).

Conflicts of Interest: The authors declare no conflict of interest.

References

1. Watzl, G.; Grünsteidl, C.; Arnoldt, A.; Nietsch, J.A.; Österreicher, J.A. In situ laser-ultrasonic monitoring of elastic parameters during natural aging in an Al-Zn-Mg-Cu alloy (AA7075) sheet. *Materialia* **2022**, *26*, 101600. [CrossRef]
2. Luo, R.; Cao, Y.; Bian, H.K.; Chen, L.L.; Peng, C.T.; Cao, F.Y.; Ouyang, L.X.; Qiu, Y.; Xu, Y.J.; Chiba, A.; et al. Hot workability and dynamic recrystallization behavior of a spray formed 7055 aluminum alloy. *Mater. Charact.* **2021**, *178*, 111203. [CrossRef]
3. Li, J.C.; Feng, D.; Xia, W.S.; Guo, W.M.; Wang, G.Y. The Non-Isothermal Double Ageing Behaviour of 7055 Aluminum Alloy. *Acta Metall. Sin.* **2020**, *56*, 1496–1508. Available online: https://www.ams.org.cn/CN/10.11900/0412.1961.2020.00039 (accessed on 15 November 2022).
4. Schreiber, J.M.; Omcikus, Z.R.; Eden, T.J.; Sharma, M.M.; Champagne, V.; Patankar, S.N. Combined effect of hot extrusion and heat treatment on the mechanical behavior of 7055 AA processed via spray metal forming. *J. Alloys. Compd.* **2014**, *617*, 135–139. [CrossRef]
5. Wu, C.H.; Feng, D.; Ren, J.J.; Zang, Q.H.; Li, J.C.; Liu, S.D.; Zhang, X.M. Effect of non-isothermal retrogression and re-ageing on through-thickness homogeneity of microstructure and properties of Al-8Zn-2Mg-2Cu alloy thick plate. *J. Cent. South Univ.* **2022**, *29*, 960–972. [CrossRef]
6. Tang, J.; Zhan, H.; Hang, H.; Teng, J.; Fu, D.F.; Jiang, F.L. Effect of Zn content on the static softening behavior and kinetics of Al–Zn–Mg–Cu alloys during double-stage hot deformation. *J. Alloys Compd.* **2019**, *806*, 1081–1096. [CrossRef]

7. Wu, C.H.; Feng, D.; Zang, Q.H.; An, S.C.; Zhang, H.; Lee, Y.S. Microstructure Evolution and Recrystallization Behavior During Hot Deformation of Spray Formed AlSiCuMg Alloy. *Acta Metall. Sin.* **2022**, *58*, 932–943. Available online: https://www.ams.org.cn/CN/10.11900/0412.1961.2021.00329 (accessed on 15 November 2022).
8. Feng, D.; Zhu, T.; Zang, Q.H.; Lee, Y.S.; Fan, X.; Zhang, H. Solution Behavior of Spray-Formed Hypereutectic AlSiCuMg Alloy. *Acta Metall. Sin.* **2022**, *58*, 1129–1141. Available online: https://www.ams.org.cn/CN/10.11900/0412.1961.2021.00079 (accessed on 15 November 2022).
9. Khan, M.A.; Wang, Y.W.; Anjum, M.J.; Yasin, G.; Malik, A.; Nazeer, F.; Khan, S.; Ahmad, T.; Zhang, H. Effect of heat treatment on the precipitate behaviour, corrosion resistance and high temperature tensile properties of 7055 aluminum alloy synthesis by novel spray deposited followed by hot extrusion. *Vacuum* **2020**, *174*, 109185. [CrossRef]
10. Liu, L.L.; Pan, Q.L.; Wang, X.D.; Xiong, S.W. The effects of aging treatments on mechanical property and corrosion behavior of spray formed 7055 aluminum alloy. *J. Alloys Compd.* **2018**, *735*, 261–276. [CrossRef]
11. Lin, X.M.; Cao, L.F.; Wu, X.D.; Tang, S.B.; Zou, Y. Precipitation behavior of spray-formed aluminum alloy 7055 during high temperature aging. *Mater. Charact.* **2022**, *9*, 112347. [CrossRef]
12. Jiang, Y.M.; Zhao, Y.; Zhao, Z.X.; Yan, K.; Ren, L.T.; Du, C.Z. The strengthening mechanism of FSWed spray formed 7055 aluminum alloy under water mist cooling condition. *Mater. Charact.* **2020**, *162*, 110185. [CrossRef]
13. Ma, S.C.; Zhao, Y.; Pu, J.H.; Zhao, Z.X.; Liu, C.; Yan, K. Effect of welding speed on performance of friction stir welded spray forming 7055 aluminum alloy. *J. Manuf. Process.* **2019**, *46*, 304–316. [CrossRef]
14. Huang, T.; Xun, J.H.; Yun, L.H.; Cheng, Y.; Hua, Y.X.; Zhang, H. Study on ductile fracture of unweldable spray formed 7055 aluminum alloy TIG welded joints with ceramic particles. *Mater. Today Comm.* **2021**, *29*, 102835. [CrossRef]
15. Feng, D.; Zhang, X.M.; Liu, S.D.; Deng, Y.L. Constitutive equation and hot deformation behavior of homogenized Al–7.68Zn–2.12Mg–1.98Cu–0.12Zr alloy during compression at elevated temperature, Mater. *Sci. Eng. A* **2014**, *608*, 63–72. [CrossRef]
16. Feng, D.; Wang, G.Y.; Chen, H.M.; Zhang, X.M. Effect of Grain Size Inhomogeneity of Ingot on Dynamic Softening Behavior and Processing Map of Al-8Zn-2Mg-2Cu alloy. *Met. Mater. Int.* **2018**, *24*, 195–204. [CrossRef]
17. Feng, D.; Zhang, X.M.; Liu, S.D.; Han, N.M. Effect of Grain Size on Hot Deformation Behavior of a New High Strength Aluminum Alloy. *Rare Met. Mater. Eng.* **2018**, *45*, 2014–2021. Available online: https://www.engineeringvillage.com/app/doc/?docid=cpx_7e3821a415743cb921fM6d3710178163171&pageSize=25&index=1&searchId=dd7704772cfb47c1bd6df21ebb694e86&resultsCount=20&usageZone=resultslist&usageOrigin=searchresults&searchType=Quick (accessed on 15 November 2022).
18. Liu, S.D.; Wang, S.L.; Ye, L.Y.; Deng, Y.L.; Zhang, X.M. Flow behavior and microstructure evolution of 7055 aluminum alloy impacted at high strain rates. *Mater. Sci. Eng. A* **2016**, *677*, 203–210. [CrossRef]
19. Yang, Q.Y.; Deng, Z.H.; Zhang, Z.Q.; Liu, Q.; Jia, Z.H.; Huang, G.J. Effects of strain rate on flow stress behavior and dynamic recrystallization mechanism of Al-Zn-Mg-Cu aluminum alloy during hot deformation. *Mater. Sci. Eng. A* **2016**, *662*, 204–213. [CrossRef]
20. Zang, Q.H.; Yu, H.S.; Lee, Y.S.; Kim, M.S.; Kim, H.W. Effects of initial microstructure on hot deformation behavior of Al-7.9Zn-2.7Mg-2.0Cu (wt%) alloy. *Mater. Charact.* **2019**, *151*, 404–413. [CrossRef]
21. Yu, H.C.; Wang, M.P.; Sheng, X.F.; Li, Z.; Chen, L.B.; Lei, Q.; Chen, C.; Jia, Y.L.; Xiao, Z.; Chen, W.; et al. Microstructure and tensile properties of large-size 7055 aluminum billets fabricated by spray forming rapid solidification technology. *J. Alloys Comp.* **2013**, *578*, 208–214. [CrossRef]
22. Feng, D.; Han, Z.J.; Li, J.C.; Zhang, H.; Xia, W.S.; Fan, X.; Tang, Z.H. Evolution Behavior of Primary Phase During Pre-heat Treatment Before Deformation for Spray Formed 7055 Aluminum Alloy. *Rare Met. Mat. Eng.* **2020**, *49*, 4253–4264. Available online: https://www.engineeringvillage.com/app/doc/?docid=cpx_5d7fe0a117788cc7620M6f6910178163190&pageSize=25&index=1&searchId=340b1898f4c045e99932ad7af2342fba&resultsCount=1&usageZone=resultslist&usageOrigin=searchresults&searchType=Quick (accessed on 15 November 2022).
23. Xiang, K.Y.; Ding, L.P.; Jia, Z.H.; Xie, Z.Q.; Fan, X.; Ma, W.T.; Zhang, H. Research progress of ultra-high strength spray-forming Al-Zn-Mg-Cu alloy. *Chin. J. Nonferrous Met.* **2022**, *32*, 1199–1224. [CrossRef]
24. Xie, Z.Q.; Jia, Z.H.; Xiang, K.Y.; Kong, Y.P.; Li, Z.G.; Fan, X.; Ma, W.T.; Zhang, H.; Lin, L.; Marthinsen, K.; et al. Microstructure evolution and recrystallization resistance of a 7055 alloy fabricated by spray forming technology and by conventional ingot metallurgy. *Metall. Mater. Trans. A* **2020**, *51*, 5378–5388. [CrossRef]
25. LI, J.C.; Wu, X.D.; Liao, B.; Lin, X.M.; Cao, L.F. Simulation of low proportion of dynamic recrystallization in 7055 aluminum alloy. *Trans. Nonferrous Met. Soc. China* **2021**, *31*, 1902–1915. [CrossRef]
26. Huang, K.; Logé, R.E. A review of dynamic recrystallization phenomena in metallic materials. *Mater. Des.* **2016**, *111*, 548–574. [CrossRef]
27. Shao, Y.; Shi, J.H.; Pan, J.C.; Liu, Q.H.; Yan, L.; Guo, P.Y. Influence of thermo-mechanical conditions on the microstructure and mechanical property of spray-formed 7055 aluminum alloy. *Mater. Today Comm.* **2022**, *31*, 103593. [CrossRef]
28. Zang, Q.H.; Chen, H.M.; Lee, Y.S.; Yu, H.S.; Kim, M.S.; Kim, H.W. Improvement of anisotropic tensile properties of Al-7.9Zn-2.7Mg-2.0Cu alloy sheets by particle stimulated nucleation. *J. Alloys Compd.* **2020**, *828*, 154330. [CrossRef]